Proceedings 10th NUMGE 2023
10th European Conference on Numerical Methods in Geotechnical Engineering
Zdravkovic L, Kontoe S, Taborda DMG, Tsiampousi A (eds)

https://doi.org/10.53243/NUMGE2023-292

Numerical investigation of the equipment set-up in triaxial testing of soft soils

C. Chao[1] , C. Jommi[1,2] , S. Muraro[1]

[1]*Department of Geoscience & Engineering, Delft University of Technology, Delft, the Netherlands*
[2] *Department of Civil and Environmental Engineering, Politecnico di Milano, Milano, Italy*

ABSTRACT: Element testing of soft soils is challenging due to the large strains attained in the pre-failure range. Besides the heterogeneity of natural samples, the set-up configuration is the main driving factor for non-homogenous response. Stress, strain and pore pressure non-uniformities induced by the loading system affect the observed behaviour and complicate proper interpretation of the results. Among the difficulties encountered in the interpretation of laboratory data, the unexpected decrease of the stress ratio frequently observed on Dutch organic soft clays on the wet side of critical state is investigated by numerically back-analysing the triaxial test set-up. A 3D finite element simulation using an advanced constitutive model for soft clays developed at TU Delft was performed to clarify the nature of the response. The results indicate that a decrease in the deviatoric stress up to critical state may be interpreted as a true feature of the soil response. However, the response at large strains is very much influenced by the triaxial shear apparatus, in particular, by the rotation of the top cap which triggers geometrical instability. Practical recommendations are given to limit the effects of the set-up configuration on the determination of the undrained shear strength to be used for field applications.

Keywords: Soft soils, Triaxial test; Constitutive modelling; Finite element simulation; Experimental set-up

1 INTRODUCTION

In the Netherlands, the stability of water defence embankments is assessed using undrained shear strength, s_u , as indicated in the WTI-2017 code of practice. To condition the interpretation of CPT tests in the field, reference s_u values are obtained from triaxial tests on undisturbed samples. However, difficulties arise in the interpretation of standard undrained triaxial tests due to the very high compressibility of the soil, which may hinder reliable use of the results for practical purposes.

Previous research has highlighted the importance of considering various aspects of the testing techniques in the interpretation of laboratory data on soft soils. Kodaka et al. (2007) studied the effects of sample shape on strain localisation of clay through both experimental testing and numerical simulations. They concluded that the deformation modes were dependent on the aspect ratio and the strain rate. The influence of end-restraint on the stress–dilatancy rule of peat was investigated by Muraro and Jommi (2019). Following Jommi et al. (2021), Zwanenburg et al. (2022) discussed the role of small and finite strain measures in the interpretation of results on soft clays.

Recent experimental investigation conducted by Gori (2020) on a typical Dutch soft silty clay, namely Gorinchem clay, found that the deviatoric stress may decrease after reaching a peak on the wet side of critical state, and that a huge reduction in the stress ratio occurs after the stress path touches the critical state line, as shown in Figure 1. The peculiar stress path observed raised questions on to which extent the observed softening response is an inherent feature of the material, in view of a reliable choice for an operative undrained shear strength.

Softening along the critical state line on the wet side has been observed previously on clays and it is often attributed to destructuration (Burland, 1990; Hight et al., 1992; Callisto & Calabresi, 1998; Cotecchia & Chandler, 2000; Pineda et al., 2016). However, Gorinchem clay shows an apparent softening response, which deviates from the critical state line and reduces the apparent mobilised shear strength to a large extent. This response was observed on loose sands too by, e.g., Goto and Tatsuoka (1988). The authors performed drained triaxial compression tests to evaluate the effects of sample slenderness and end kinematic conditions on samples of loose Toyoura sand and found that the reduction in stress after peak largely depends on the rotation of the load cap. Following these results, Mozaffari et al. (2022) suggested that properties of sands can be obtained more reliably by using fixed cap in the triaxial equipment.

A combination of laboratory tests and numerical simulations is presented in the following, to analyse the observed response of Gorinchem clay and assess the influence of the triaxial set-up on the material response.

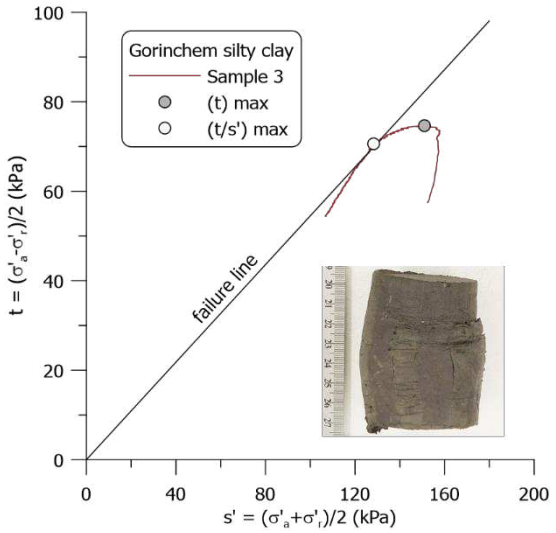

Figure 1. Stress path and picture of one sample of NC Gorinchem silty clay at the end of ACU tests from Gori (2020)

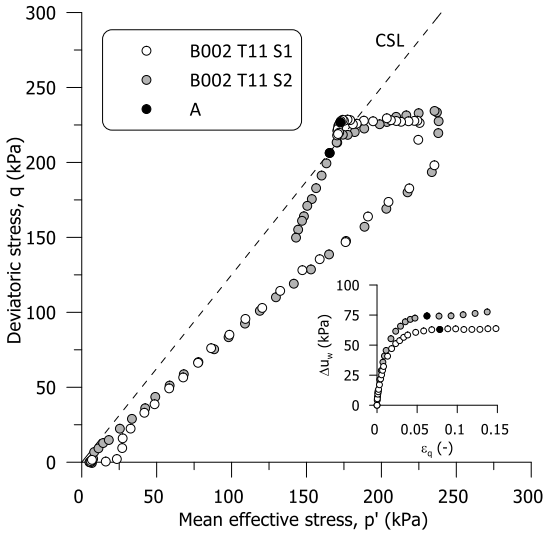

Figure 2. ACU stress paths and excess pore pressure of specimen B002 T11 S1 and B002 T11 S2

Figure 3. Pictures of the two specimens at the end of the test

2 EXPERIMENTAL OBSERVATION

Although research suggests that using fixed cap and smooth platens guarantees more accurate results in triaxial tests, rotating caps and rough platens are still commonly used in practice (e.g., Reid et al., 2021). The triaxial tests conducted for this study also employed rotating caps and rough platens to replicate the reference testing conditions. The tests were conducted on undisturbed organic silty clay samples retrieved at a depth of 4.7 m NAP, from a borehole (B002) starting from the crest of the Maasdijk near Oijen in the Netherlands. The specimens had a height-to-diameter ratio of 2.5, and were consolidated under K_0 conditions to σ'_v= 375 kPa before undrained shear at a constant strain rate of 0.015%/min. The pore water pressure during the tests was measured at the bottom of the specimens. As a preliminary choice, the equivalent cylinder area correction was applied in processing the experimental data. The results of the two tests are discussed in the following.

Among the tested specimens, one (B002 T11 S2) showed the same softening response as Gorinchem silty clay, and its stress path in p'-q space deviated from the critical state line after reaching the critical state stress ratio (point A), as shown in Figure 2. In the same figure, the development of excess pore pressure is also reported, which shows the attainment of an almost constant value beyond point A. Inspection of the specimens after testing (Figure 3) revealed that the failure mode of B002 T11 S2 was different from B002 T11 S1, and characterised by buckling-like deformation with a single plane localization and rotation of the top part of the specimen. Based on the experimental observation we investigated whether the observed behaviour could be just a consequence of the top and bottom caps kinematic restraint, by means of a numerical analysis.

3 NUMERICAL SIMULATIONS

3.1 Coupled hydro-mechanical 3D finite element analysis

Coupled hydro-mechanical 3D finite element analyses were performed in ABAQUS to study the influence of the apparatus set-up on the observed response. The simulations were conducted using the model shown in Figure 4, including the top cap and the soil specimen. Two different H/D ratios were used in the simulations, and the kinematic condition of the top cap was left either fixed or free-to-rotate. A contact pair with rough tangential behaviour was adopted for the interaction between the top cap and the specimen, to replicate the experimental set-up as much as possible. The initial stress state reproduced at the start of the numerical simulations was the one at the end of anisotropic consolidation under K_0 conditions. The final undrained shearing stage was simulated by imposing no drainage at the top and bottom of the sample.

An additional simulation with a much finer mesh of the soil specimen was performed to evaluate the well-known mesh dependency in numerical simulations.

The H/D ratio, number of elements, and kinematic condition imposed at the top cap are summarised in Table 1 for each simulation. The undrained triaxial compression was simulated by imposing the same strain rate at the top centre of the cap until the axial strain reached 30%, replicating a suggested practice in the Netherlands. The top cap was modelled as an elastic material having Young modulus E = 1000 GPa and Poisson ratio ν = 0.33.

The soil response was described using a fully non-associate elastic-plastic constitutive model recently developed at TU Delft, to better replicate the response of organic soft clays. The model adopts the generalised yield function proposed by McDowell and Hau (2004), to replicate the shape of the yield locus detected experimentally, and Dafalias et al. (2006) formulation for anisotropy. Evolution of anisotropy in the model is described by an amended version of the rotational hardening rule by Dafalias and Taiebat (2013). The constitutive model was implemented in ABAQUS via a UMAT subroutine.

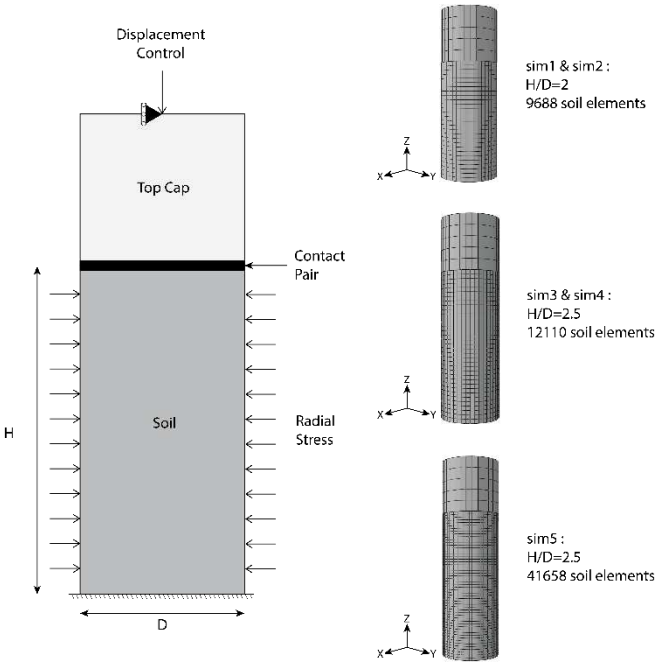

Figure 4. 3D finite element models in ABAQUS

Table 1. H/D ratio, number of elements, and kinematic condition of top cap for each simulation

ID	H/D	No. of elements (top cap/soil)	Kinematic condition of top cap
sim1	2.0	925/9688	Fixed
sim2	2.0	925/9688	Free-to-rotate
sim3	2.5	925/12110	Fixed
sim4	2.5	925/12110	Free-to-rotate
sim5	2.5	925/41658	Free-to-rotate

3.2 Calibration of model parameters

The model requires the calibration of the nine parameters listed in Table 2. The log-log compression parameters κ^* and λ^* were obtained from the K_0 path on test B002 T11 S1. The critical state stress ratio, M_g, the two parameters describing the shape of the yield locus (M_f, k_f) and the Poisson ratio ν were taken from a large data set on organic silty clay from a parallel study. The last three parameters, z, s, c, describe the rotational hardening rule. The two parameters z and s were determined from the data of K_0 compression, following the approach of Dafalias et al. (2013). The initial calibration was refined to best capture the undrained compression paths. Eventually, the model parameters used in the simulation are reported in Table 2. The hydraulic conductivity was set to $2 \cdot 10^{-9}$ m/s.

Table 2. Calibrated model parameters used in the analyses

Parameter	Description	Value
M_g	critical state stress ratio	1.25
λ^*	slope of compression line on ln v–ln p' plane	0.053
κ^*	slope of rebound line on ln v–ln p' plane	0.006
ν	Poisson's ratio	0.2
c	rate of evolution of anisotropy	50
s	saturation limit of anisotropy	1.43
z	saturation limit of anisotropy	1.43
M_f	shape of the yield surface	1
k_f	shape of the yield surface	1.5

Three state variables (e_0, p'_0, α_0) are needed to initialise the model. The initial void ratio e_0 can be easily obtained from the experimental information. The initial inclination of the yield surface and plastic potential, α_0, was determined assuming K_0 conditions in the field, based on the ratio between the volumetric and deviatoric strain increment (Dafalias et al., 2006):

$$\alpha = \frac{B\varepsilon\eta_{K_0}^3 + \eta_{K_0}^2 + \left[2(1-\kappa^*/\lambda^*) - BM_g^2\right]\varepsilon\eta_{K_0} - M_g^2}{2\varepsilon(1-\kappa^*/\lambda^*)} \quad (1)$$

where

$$B = -\frac{2(1+\nu)}{9(1-2\nu)}\frac{\kappa^*}{\lambda^*} \quad , \quad (2)$$

η_{K0} is the stress ratio corresponding to $K_0^{NC} = 0.46$, and $\varepsilon = 3/2$. Given that the samples were consolidated above the pre-consolidation pressure in the field, the inclination of the yield surface and plastic potential α_0 at saturation were calculated from the parameters in Table 2. The corresponding pre-consolidation pressure p'_0 is obtained with the stress state before undrained shearing and α_0. The model simulation as a single Gauss point for test B002 T11 S1 is shown in Figure 5.

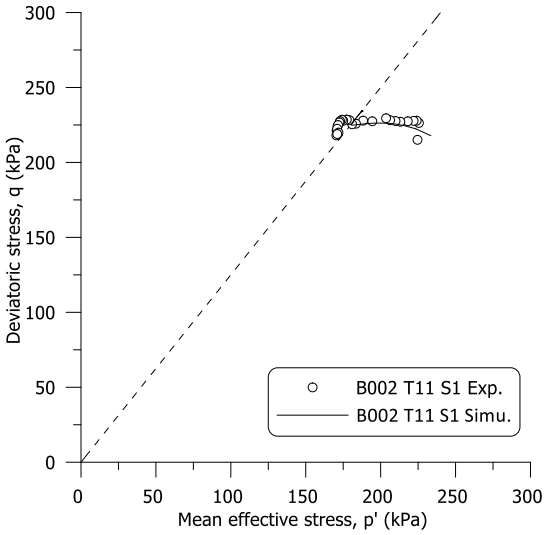

Figure 5. Single Gauss point simulation and experimental data of B002 T11 S1

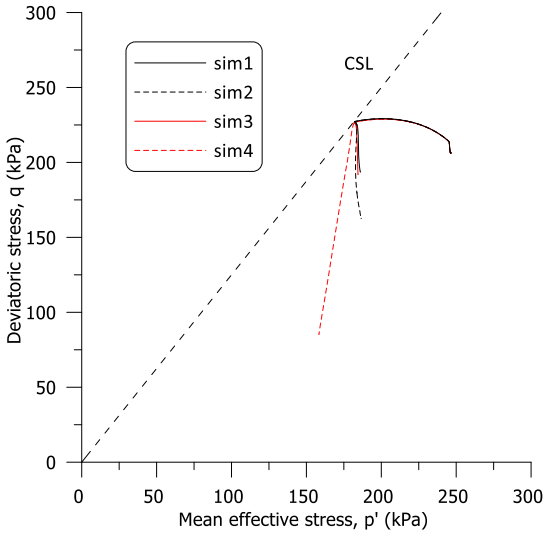

Figure 6. Stress path calculated from sim1 to sim 4

3.3 *Finite Element results*

Results of the FE simulations are presented in terms of global quantities, with the axial stress calculated from the reaction force at top centre of the cap with the area correction of an equivalent cylinder. The excess pore water pressure is obtained by averaging the value of the elements at the bottom boundary of the FE model.

Figure 6 presents the stress paths obtained in the simulations from 1 to 4. As expected, all simulations predict the same stress path before reaching the critical state. However, the stress paths deviate after they reach CSL and show softening response. With reference to Figure 7, it can be noticed that sim1 and sim3 predict a barrelling failure mode, while sim2 and sim 4 predict a buckling-like failure mode with substantial rotation of the top part of the specimen following the top cap.

The results of the simulations show that increasing the height to diameter ratio from H/D = 2 to H/D = 2.5 helps in reducing localised bulging caused by end-restraint. However, when buckling failure mode is observed (sim2 and sim4) increasing the height-to-diameter ratio exacerbates strain localisation, which results in a larger reduction of the mobilised stress ratio.

It is worth mentioning that strain localisation in the simulations was not forced in any way. End friction at the top and bottom caps and numerical round-off errors were enough to generate the observed non-uniform failure modes.

The check performed to evaluate the influence of the element size on the results is shown in Figure 8. Reducing the element size reduces the size of the localised shear band, as expected. However, the stress path is not affected substantially by the element size.

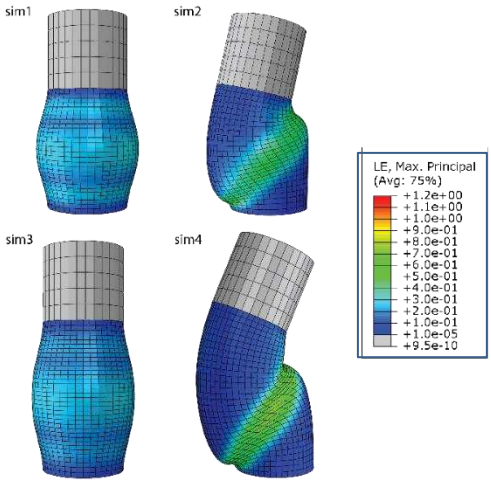

Figure 7. Failure mode of sim1 to sim4

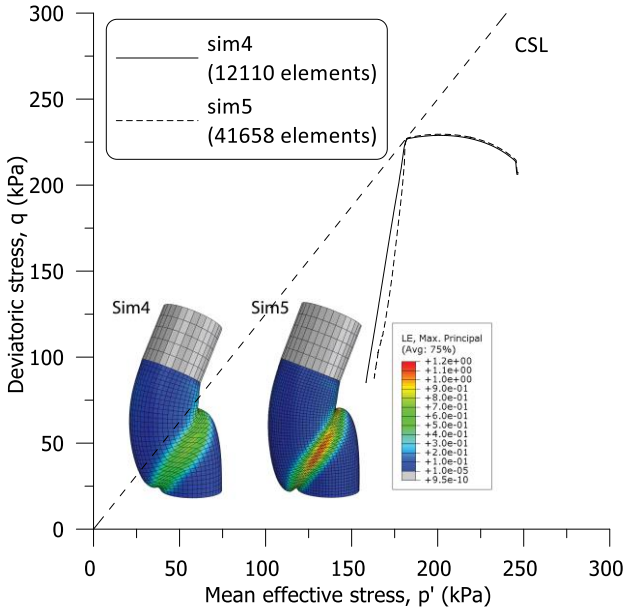

Figure 8. Influence of the element size on the stress path calculated from sim4 and sim5 and failure mode at the end of undrained shearing

4 DISCUSSION

The experimental data and the results of the numerical simulations are presented together in Figure 9. The simulation results match well the experimental data before reaching critical state and capture the following trend nicely (Figure 9(a)). The difference in the last part of the computed stress path comes from slight under estimation of the excess pore water pressure in the simulations. The deviatoric stress-strain responses are plotted in Figure 9(b) together with the model prediction of the single Gauss point. The latter shows that a reduction in the deviatoric stress below the critical state stress ratio may occur due to the non-associated soil response. However, the reduction in the stress ratio after reaching critical state is a feature coming from the non-homogeneous sample response and can be reproduced only in the FE analysis, though using the same model for the soil.

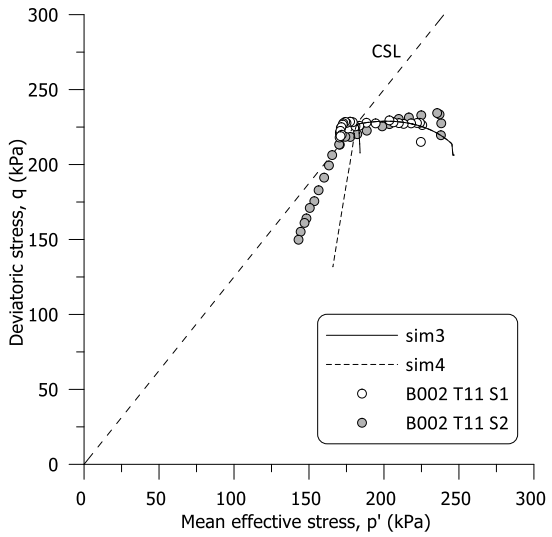

(a)

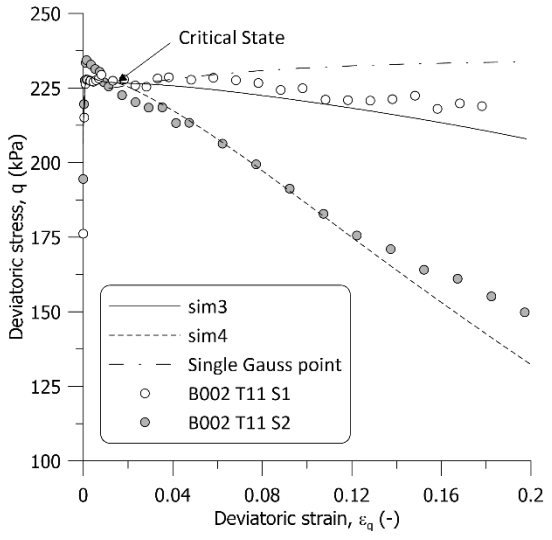

(b)

Figure 9. Comparison between experiments and simulations (a) stress path (b) deviatoric strain-stress relation

If the interaction between the cap and the soil specimen is taken into account, the numerical simulations align well with the experimental observation. The failure modes predicted numerically resemble well the ones detected experimentally.

Figure 10 presents the variation of the reaction forces at top centre of the cap for sim3 and sim4. When the cap rotates (sim4), the axial force decreases while non null horizontal force components arise. To further inspect the relevance of standard procedures in elaborating experimental data, the relevance of the choice on the area correction is briefly discussed with reference to Figure 11.

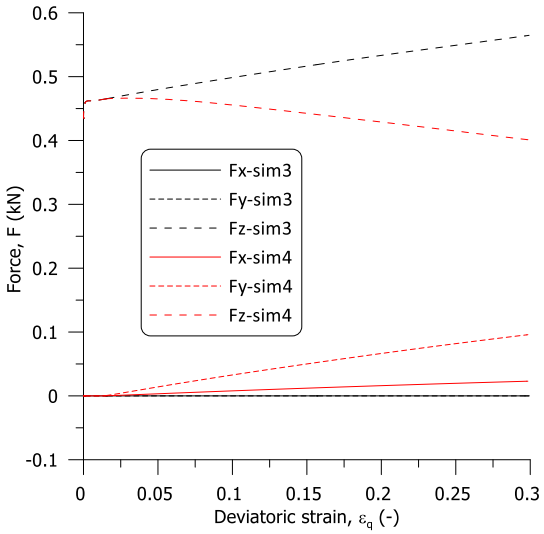

Figure 8. Components of the reaction force at top cap for sim3 and sim4

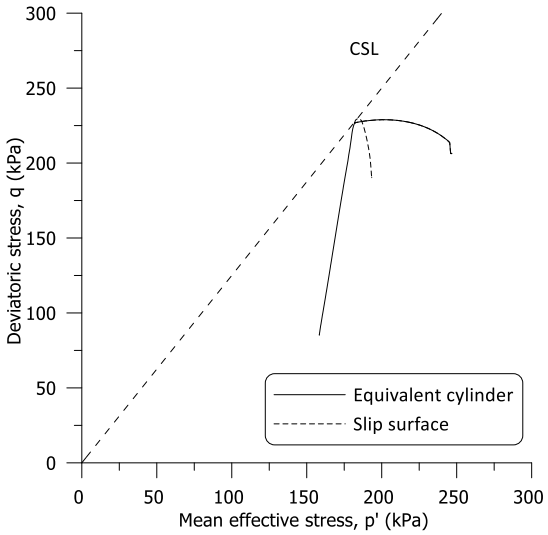

Figure 91. Stress paths derived from sim4 with different area correction assumptions

The stress paths obtained from sim4 with two different approaches, namely the equivalent cylinder and inclusion of slip surface (Head, 1998), are presented in the figure. The area correction for a slip surface shows a less drastic softening response and an opposite

trend for pore pressure after critical state. Actually, the failure modes observed experimentally are usually hybrid. Sample B002 T11 S1 resembles a barrel, but with some localised strains around mid-height. In sample B002 T11 S2 the shear band is not as localised as the theory would suggest. In both cases, the last state, which can be truly associated to the material behaviour, is the stress state at critical state.

5 CONCLUSIONS

The work was meant to provide a contribution to the choice of a reliable undrained shear strength reference for practical applications of interest for Dutch organic soft clays. The combination between the experimental tests and the numerical analyses allowed concluding that the peculiar behaviour, frequently interpreted as "softening", may not derive from true softening of the soil. On the one hand, the decrease in the deviatoric stress before reaching critical state is due to the non-associated response of these type of soils. The post-critical state reduction in the stress ratio, on the contrary, is mostly a result of typical triaxial set-up.

The bias cannot be solved easily at the experimental level, as two contradictory suggestions for the triaxial set-up would emerge from the conclusions of this work. Taller samples (high H/D ratio) allow reducing the influence of the shear stresses at the top and bottom caps on the response. However, increasing the H/D ratio increases the susceptibility of the sample to bending instability. To accommodate both requirements, smooth top and bottom caps with no-rotation seems the best option.

For practical purposes, it is suggested to avoid using the maximum deviatoric stress reached during the test to infer the undrained shear strength. The deviatoric stress at critical state is a better and more reliable estimate of the true material shear strength. The decrease in the deviatoric stress observed before reaching critical state may occur due to non-associated yield surface and plastic potential, without any "destructuration" being enforced in the model. The post-critical decrease in the stress ratio can be a mere artefact of the experimental equipment, when rough bases and rotating caps are adopted.

6 ACKNOWLEDGEMENT

The financial contribution of NWO on the project SOFTTOP DEEP.NL.2018.006 is gratefully acknowledged.

7 REFERENCES

Burland, J. 1990. On the compressibility and shear strength of natural clays. *Géotechnique,* **40**(3), 329-378.

Callisto, L., & Calabresi, G. 1998. Mechanical behaviour of a natural soft clay. *Géotechnique,* **48**(4), 495-513.

Cotecchia, F., & Chandler, R. 2000. A general framework for the mechanical behaviour of clays. *Géotechnique,* **50**(4), 431-447.

Dafalias, Y. F., & Taiebat, M. 2013. Anatomy of rotational hardening in clay plasticity. *Géotechnique,* **63**(16), 1406-1418.

Dafalias, Y. F., Manzari, M. T., & Papadimitriou, A. G. 2006. SANICLAY: simple anisotropic clay plasticity model. *International Journal for Numerical and Analytical Methods in Geomechanics,* **30**(12), 1231-1257.

Gori, A. 2020. *The unexpected softening of the undrained shear strength of organic and silty clays in Rhine delta: a conceptual study.* MSc thesis, TU Delft, The Netherlands.

Goto, S., & Tatsuoka, F. 1988. Effects of end conditions on triaxial compressive strength for cohesionless soil. In *Advanced triaxial testing of soil and rock*: ASTM International.

Head, K. H. 1998. *Manual of soil laboratory testing. Volume 3: effective stress tests*: John Wiley & Sons.

Hight, D., Bond, A., & Legge, J. 1992. Characterization of the Bothkennaar clay: an overview. *Géotechnique,* **42**(2), 303-347.

Jommi, C., Chao, C., Muraro, S., & Zhao, H. 2021. Developing a constitutive approach for peats from laboratory data. *Geomechanics for Energy and the Environment,* **27**, 100220.

Kodaka, T., Higo, Y., Kimoto, S., & Oka, F. 2007. Effects of sample shape on the strain localization of water-saturated clay. *International Journal for Numerical and Analytical Methods in Geomechanics,* **31**(3), 483-521.

McDowell, G., & Hau, K. 2004. A generalised modified cam clay model for clay and sand incorporating kinematic hardening and bounding surface plasticity. *Granular Matter,* **6**(1), 11-16.

Mozaffari, M., Liu, W., & Ghafghazi, M. 2022. Influence of specimen nonuniformity and end restraint conditions on drained triaxial compression test results in sand. *Canadian Geotechnical Journal,* **99**(999), 1-13.

Muraro, S., & Jommi, C. 2019. Implication of end restraint in triaxial tests on the derivation of stress–dilatancy rule for soils having high compressibility. *Canadian Geotechnical Journal,* **56**(6), 840-851.

Pineda, J., Suwal, L., Kelly, R., Bates, L., & Sloan, S. 2016. Characterisation of Ballina clay. *Géotechnique,* **66**(7), 556-577.

Reid, D., Fourie, A., Ayala, J. L., Dickinson, S., Ochoa-Cornejo, F., Fanni, R., . . . Ovalle, C. 2021. Results of a critical state line testing round robin programme. *Géotechnique,* **71**(7), 616-630.

Zwanenburg, C., Teunissen, H., & Konstantinou, M. 2022. Small and large strain approach in triaxial testing. *Proceedings of the 20th International Conference on Soil Mechanics and Geotechnical Engineering,* 291-296, Sydney.